The Mutual Coupling and Diffraction Effects on the Performance of a CMA Adaptive Array

Hao Yuan, Kazuhiro Hirasawa, *Member, IEEE,* and Yimin Zhang

***Abstract*—The performance of the constant modulus algorithm (CMA) with the steepest descent method used in an adaptive array of monopole antennas mounted on a rectangular conducting plate was investigated. The mutual coupling (MC) effect among the array elements and the diffraction effect caused by the conducting plate were taken into account in the calculation by a hybrid method of moment method (MM) and geometrical theory of diffraction (GTD). Simulations showed that the CMA adaptive array performs differently when the MC and the diffraction effects are taken into account. In some cases, the speed of convergence is slower with MC, and in other cases it is faster. Also, in multipath scenarios the array sometimes converges on a weaker delayed ray rather than the direct ray when MC is included. The capture property is explained by the fact that the CMA algorithm is sensitive to initial conditions and the initial array pattern is directional due to MC—not omnidirectional as in the ideal case. The performance of the array on a finite ground plane is different from that on an infinite ground plane due to diffraction effects.**

***Index Terms*— Adaptive array, constant modulus algorithm, finite conducting plane, monopole, mutual coupling.**

I. Introduction

THE CONSTANT modulus algorithm (CMA) was first proposed by Treichler *et al.* in 1983 [1]. The algorithm can compensate for both frequency-selective multipath and interference on modulated signals with a constant envelope such as frequency- and phase-modulated carriers. The method employs only *a priori* knowledge of the constant envelope about the transmitted signal waveform, which is often the case in a real communication environment. The method exploits the fact that multipath reception and various interference sources generate incidental amplitude fluctuations on the received signal and makes use of this point to suppress the multipath rays and interferences. It resembles the least-mean squares (LMS) algorithm [2], but it has the advantage that no external "desired" signal is required for the operation of the algorithm.

Gooch *et al.* applied the CMA to array antennas and formed the CMA adaptive array in 1986 [3], where they analyzed the directionality and the capture property of the CMA adaptive array. Fujimoto *et al.* combined the CMA adaptive array with the Marquardt method in 1991 [4]. In their paper, it is shown that the convergence rate of the CMA with the Marquardt method for optimization is much faster than that of the CMA with a steepest descent method.

Although the performance of a CMA adaptive array has been analyzed in various aspects, the analyses have been based on the assumption that the array elements are omnidirectional and in free space. Not only the mutual coupling (MC) effects among the array elements, but also the characteristics of the array element itself have not yet been taken into account in the simulation, but in a real communication environment, the directional antennas are used and mounted on a metal support. Because of the space limitation, the MC among the array elements becomes significant, and this will distort the array patterns [5]. So it is important to consider the MC effects among the array elements and the effects of diffraction caused by the support in the analysis.

In this paper, the performance of a CMA adaptive array with the steepest descent method is investigated. The MC effects among the array elements are taken into account by using the moment method (MM) when the array is placed on an infinite ground plane. Furthermore, a more practical situation is considered, where the array is mounted on a rectangular conducting plate, which may be a model of setting the array on the roof of a car or on the top of an antenna tower. The diffraction effects due to the edges of the conducting plate are taken into account by using the hybrid method of MM and geometrical theory of diffraction (GTD). In Section II, the CMA adaptive array is described briefly. In Section III, the computational method used in the simulation is presented. In Section IV-A, the performance of a CMA adaptive array with the consideration of MC when placed on an infinite ground plane is investigated first for two-ray incidence. Then, an example of three-ray incidence is given to show that the CMA adaptive array can also suppress the delayed rays more than one with MC. In Section IV-B, the performance of the CMA adaptive array on a rectangular conducting plate is analyzed and compared with that on the infinite ground plane. It shows that the diffracted field caused by the edges of the finite plate can also affect the convergent speed and the capture property of the CMA adaptive array.

II. The CMA Adaptive Array

A CMA adaptive array is an adaptive system suitable for mobile communication, where it can successfully suppress interference under a multipath environment. Fig. 1 shows a diagram of an N element adaptive array, where complex $X_i(t)$ is the output of the ith antenna element, while $X_i(k)$

Manuscript received December 15, 1995; revised November 11, 1996.

H. Yuan is with the Kyocera DDI Institute of Future Telecommunications, Inc., Tokyo 150-0001, Japan (e-mail: yuan@kdi.co.jp).

K. Hirasawa is with the Institute of Information Sciences and Electronics, University of Tsukuba, Tsukuba 305, Japan.

Y. Zhang is with the Communication Laboratory, Japan Corporation, Kawasaki 213, Japan.

Publisher Item Identifier S 0018-9545(98)02476-1.

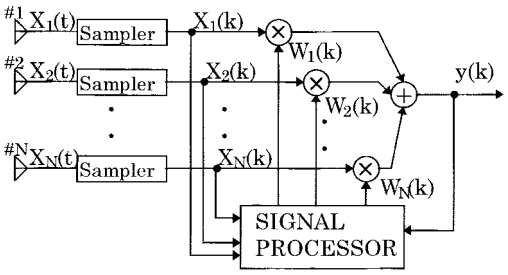

Fig. 1. The diagram of an N element adaptive array.

is the system input at the kth sampling instant and it is a multipath distorted constant modulus signal. $W_i(k)$ is the complex weight at the ith antenna element. The system output at the kth sampling instant $y(k)$ can be written as

$$y(k) = \boldsymbol{W}^T(k)\boldsymbol{X}(k) \tag{1}$$

where

$$\boldsymbol{X}(k) = [X_1(k) \quad X_2(k) \quad \cdots \quad X_N(k)]^T$$

is the vector of the system input and

$$\boldsymbol{W}(k) = [W_1(k) \quad W_2(k) \quad \cdots \quad W_N(k)]^T$$

is the vector of adjustable weights. The superscript T denotes transpose.

The CMA adaptive array eliminates the amplitude fluctuations of the array output due to the existence of the interferences. The cost function to be minimized can generally be expressed as

$$J_{pq}(\boldsymbol{W}) = E[||y(k)|^p - \sigma^p|^q] \tag{2}$$

where p and q are positive integers. $E[\cdot]$ denotes the expectation and σ is the amplitude of the array output in the absence of interference. To minimize the cost function, the steepest descent method is employed for optimization. The weight vector which adjusts the output of the array is updated according to the following:

$$\boldsymbol{W}(k+1) = \boldsymbol{W}(k) - \mu\nabla_{\boldsymbol{W}} J_{pq}[\boldsymbol{W}(k)] \tag{3}$$

where μ is a positive step size and $\nabla_{\boldsymbol{W}}$ is the gradient operator with respect to the element of the vector $\boldsymbol{W}$.

In this paper, p and q are chosen to be two. Then, $\nabla_{\boldsymbol{W}} J_{pq}[\boldsymbol{W}(k)]$ can be expressed as follows:

$$\nabla_{\boldsymbol{W}} J_{2,2}[\boldsymbol{W}(k)] = 4E\{[|y(k)|^2 - \sigma^2]\boldsymbol{X}^*(k)y(k)\} \tag{4}$$

where the superscript * denotes a complex conjugate.

III. The Computational Method

1) The Cost Function and the Step Size: Since we cannot obtain exactly the ensemble mean from the finite data of a series, the expectation symbol must be removed from the updated equation. An average of a finite number of data samples is used to replace the ensemble mean. Then, the cost function for $p = q = 2$ becomes

$$J(W) = \frac{1}{L}\sum_{i=k}^{k+L-1}[||y_i(k)|^2 - \sigma^2|^2] \tag{5}$$

where L is the number of data and

$$y_i(k) = \boldsymbol{W}^T(k)\boldsymbol{X}(i). \tag{6}$$

It should be noted that in (5) the system input vector $\boldsymbol{X}(i)$ is sampled at the instant i, where i varies from k to $k+L-1$, while the weight vector keeps the constant value at the instant k. With this substitution for the cost function, the weight updated (3), combined with (4), becomes

$$W(k+1) = W(k) - \frac{4\mu}{L}\sum_{i=k}^{k+L-1} \cdot \{[|y_i(k)|^2 - \sigma^2]X^*(i)y_i(k)\}. \tag{7}$$

This means that L data are used for one update of weight vector $\boldsymbol{W}$. With this updated equation, the weight vector is calculated one by one.

The step size μ in (7) is chosen as [6]

$$\mu = 1\Big/\left[\frac{1}{L}\sum_{i=k}^{k+L-1} 6\lambda_{\max}^2(i)\right] \tag{8}$$

where $\lambda_{\max}(i)$ is the maximum eigenvalue of the correlation matrix $\boldsymbol{X}^*(i)\boldsymbol{X}^T(i)$. With this step size, the algorithm has the fastest speed of convergence.

2) The MC Effects and Diffracted Field: When we take into account MC effects among the array elements and the diffracted field caused by the conducting plate in the calculation, the current vector on the array elements $\boldsymbol{I}$ can be numerically calculated by the hybrid method of MM and GTD from the following matrix equation [7]:

$$\boldsymbol{ZI} = \boldsymbol{V} \tag{9}$$

where $\boldsymbol{Z}$ is the generalized impedance matrix and $\boldsymbol{V}$ is the induced voltage vector due to the incident field. The mnth element of the matrix $\boldsymbol{Z}$ and the mth element of the vector $\boldsymbol{V}$ are given as

$$Z_{mn} = Z'_{mn} + Z^l_{mn} + Z^g_{mn} \tag{10}$$

and

$$V_m = V'_m + V^g_m \tag{11}$$

where

$$Z'_{mn} = -\int_{lm} \boldsymbol{W_m}\cdot\boldsymbol{E^s_n}\,dl \tag{12}$$

and

$$V'_m = \int_{lm} \boldsymbol{W_m}\cdot\boldsymbol{E^i}\,dl \tag{13}$$

where l_m is the segment on which the mth expansion function is located. $\boldsymbol{W_m}$ is the mth testing function. Here, the piecewise sinusoidal function is used for both the expansion function and the testing function. $\boldsymbol{E^s_n}$ is the scattered field from the nth current expansion function per unit current, and $\boldsymbol{E^i}$ is the incident field. Z^l_{mn} $(n = m)$ is the lumped load impedance corresponding to the output terminal of each element of the array, where Z^l_{mm} is connected ($Z^l_{mn} = 0$ when $n \neq m$ or m is not equal to the number of the expansion function

at the output terminal of the antenna elements). Z_{mn}^{g} is the component of the impedance caused by the diffracted field of $\boldsymbol{E_n^s}$ due to the edges of the conducting plate. Here, the corner diffraction is ignored because it is very weak when the distance between the antenna and corner are larger than 0.3λ [8]. V_m^g is the voltage component due to the diffracted field of the incident field. Thus, Z_{mn}^{g} and V_m^g can be written as

$$Z_{mn}^{g} = -\int_{lm} \boldsymbol{W_m} \cdot \boldsymbol{E_n^{sg}}\, dl \tag{14}$$

and

$$V_m^g = \int_{lm} \boldsymbol{W_m} \cdot \boldsymbol{E^{ig}}\, dl \tag{15}$$

where $\boldsymbol{E_n^{sg}}$ and $\boldsymbol{E^{ig}}$ are, respectively, the diffracted fields of $\boldsymbol{E_n^s}$ and $\boldsymbol{E^i}$ due to the edges of the rectangular conducting plate. $\boldsymbol{E_n^{sg}}$ and $\boldsymbol{E^{ig}}$ can be calculated by GTD.

To calculate $\boldsymbol{E_n^{sg}}$ and $\boldsymbol{E^{ig}}$, the following formula is used [9], [10]:

$$\begin{bmatrix} E_{//}^{d}(s) \\ E_{\perp}^{d}(s) \end{bmatrix} = \begin{bmatrix} -D_{//} & O \\ O & -D_{\perp} \end{bmatrix} \begin{bmatrix} E_{//'}^{i}(Q) \\ E_{\perp'}^{i}(Q) \end{bmatrix} A(s) e^{-j\beta s} \tag{16}$$

where $\boldsymbol{E_{//}^{d}}(s)$ and $\boldsymbol{E_{\perp}^{d}}(s)$ are the diffracted field components parallel and perpendicular to the plane of diffraction, respectively. $\boldsymbol{E_{//'}^{i}}(Q)$ and $\boldsymbol{E_{\perp'}^{i}}(Q)$, which are, respectively, parallel and perpendicular to the plane of incidence, are the two components of the incident field in the immediate neighborhood of the diffraction point Q. $D_{//}$ and $D_{\perp}$ are the scalar diffraction coefficients associated, respectively, with the parallel and perpendicular field component, which are dependent upon the type of incident wave and the angle of incidence. $\boldsymbol{s}$ is the distance between the diffraction point and the observation point. $A(s)$ is the spatial attenuation factor defined as

$$A(s) = \begin{cases} 1/\sqrt{s}, & \text{for plane wave incidence} \\ \{s'/[s(s'+s)]\}^{1/2}, & \text{for spherical wave incidence} \end{cases} \tag{17}$$

where $\boldsymbol{s'}$ is the distance between the source point and the diffraction point. $\beta = 2\pi/\lambda$ is the wave number in the free space. λ is the wavelength of operation.

For $\boldsymbol{E_n^{sg}}$ and $\boldsymbol{E^{ig}}$, spherical wave incidence and plane wave incidence are assumed, respectively. $\boldsymbol{E_{//'}^{i}}(Q)$ and $\boldsymbol{E_{\perp'}^{i}}(Q)$ can be obtained from $\boldsymbol{E_n^s}$ for Z_{mn}^{g} by using the *three-point source formula* [8], [11], and for V_m^g, they can be obtained from $\boldsymbol{E^i}$.

When the current on the elements of the array is calculated from (9), the element output voltage $X_i(t)(i = 1, 2, \cdots, N)$ can be obtained by the multiplication of the current at the output terminal by the corresponding load impedance.

With (16), the receiving patterns of a $\lambda/4$ monopole on a finite square conducting plate have been calculated, and they are consistent with the radiation pattern of [12, Fig. 11.36] and that of [13, Fig. 5].

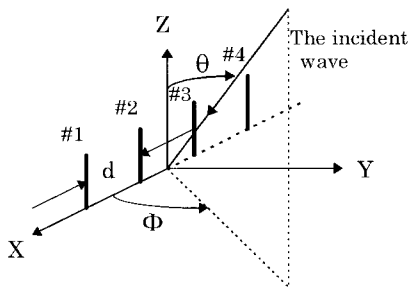

Fig. 2. The configuration of the linear array with four equally spaced quarter-wavelength monopoles on an infinitely large ground plane.

IV. The Simulation

A. CMA Adaptive Array on an Infinitely Large Ground Plane [14]

1) Array Parameters: The purpose of this section is to compare the performance between the CMA adaptive array with and without the consideration of MC effects among the array elements when the array is placed on an infinitely large ground plane.

As an example, an equally spaced linear array with four quarter-wavelength monopoles is considered (Fig. 2). The radius of each monopole is 0.002λ.

In the calculation, it is assumed that the rays come from the horizontal direction. The angle Φ denotes the incoming direction of the ray, and $\boldsymbol{d}$ is the interelement spacing. The pseudo-noise (PN) code produced by a ten-stage shift register generator of maximal period sequence is used to generate a $\pi/4$ shift QPSK signal with a symbol duration T. The incident wave is assumed to be a plane wave modulated by a $\pi/4$ shift QPSK signal, which has the following form:

$$\boldsymbol{E} = \boldsymbol{E_\theta} \exp(-j\boldsymbol{k} \cdot \boldsymbol{r}) \exp\{j[\omega t + \varphi(t)]\} \tag{18}$$

where $\boldsymbol{E_\theta}$ is the electric field amplitude in the $\boldsymbol{\theta}$ direction and $(\boldsymbol{r}, \boldsymbol{\theta}, \boldsymbol{\Phi})$ is a spherical coordinate system. $\boldsymbol{k}$ is the wave number vector, and $\boldsymbol{r}$ is the vector of the observation point. ω is the angular frequency, and $\varphi(t)$ is the $\pi/4$ shift QPSK signal, which has the form as

$$\varphi(t) = \varphi_k = \varphi_{k-1} + \Delta\varphi_k \quad kT \le t < (k+1)T \tag{19}$$

where $\Delta\varphi_k = \pm\pi/4, \pm 3\pi/4$. For simplicity, the signal bandwidth is not considered in the computation. Each antenna is terminated by a 50-Ω load, and the MC effects among the array elements are considered by MM. In the calculation, 15 snapshots are used to update the weight vector [i.e., $L = 15$ in (5)]. Each snapshot is taken at the center of a symbol of the first arriving signal. For a cost function, let $\sigma = 1$ and the initial weight vector is set to be $W_0 = [1, 0, 0, 0]^T$. Since all the output powers of the antenna elements are not the same anymore when MC effects are taken into account, the signal-to-noise ratio (SNR) is defined as the ratio of the power at the receiving terminal of the first element of the array to that of thermal noise and set to be 40 dB. The electric field amplitude ratio of the first to the second incident ray is 3 dB, and the time delay of the second ray is T compared with the first one.

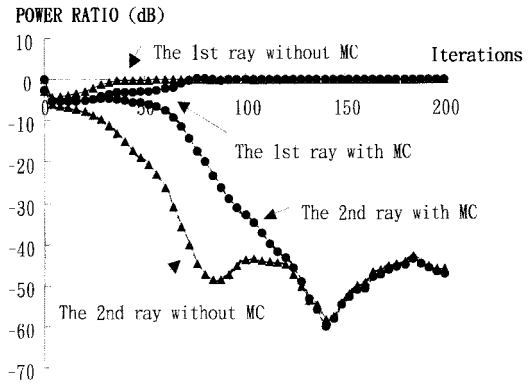

Fig. 3. The output power with respect to the number of iterations with and without MC, where $\Phi_d = 90°$, $\Phi_i = 60°$, and $d = 0.5\lambda$.

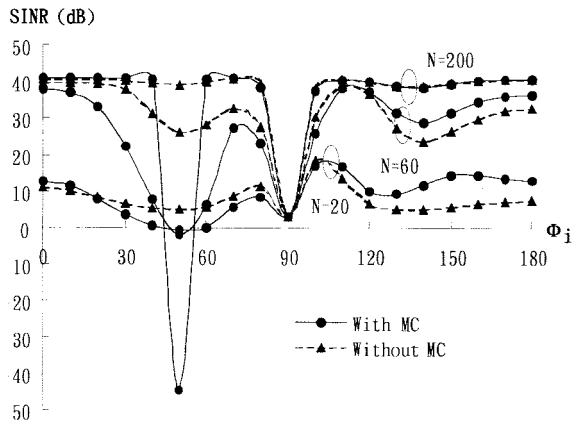

Fig. 4. The intermediate SINR patterns with respect to Φ_i when $\Phi_d = 90°$ and $d = 0.5\lambda$.

2) The Array on the Infinite Ground Plane with Two-Ray Incidence: Assume that the first and second (delayed) ray come from $\Phi_d = 90°$ and $\Phi_i = 60°$, respectively. Fig. 3 shows the array output power normalized by the initial output power of the first ray with and without MC. The interelement spacing $\boldsymbol{d}$ is set to be $\lambda/2$. Although CMA converges with and without MC, the speed of convergence with MC is slower than that without MC. Fig. 4 shows the intermediate desired signal-to-interference-plus-noise ratio (SINR) patterns, with and without MC, when $\Phi_d = 90°$ and Φ_i varies from 0° to 180°. (Here, we consider the delayed ray as the interference signal.) The number of iterations is set to $N = 20$, 60, and 200. It can be seen that when $\Phi_i > 120°$, the speed of convergence with MC is faster than that without MC, while when $\Phi_i < 90°$, the result is reversed. After 200 iterations, the two patterns are almost the same except at $\Phi_i = 50°$, where the SINR without MC is about 39 dB. This means that the CMA adaptive array has caught the first ray. On the other hand, when with MC, the SINR is -45 dB, since the array has caught the second ray. The reason is that when MC is taken into account, the initial receiving pattern with the initial weight vector $W_0 = [1, 0, 0, 0]^T$ is not omnidirectional any more. It has a maximum value when $\Phi = 50°$ while the initial receiving pattern without MC is isotropic. Fig. 5 shows the SINR patterns with and without

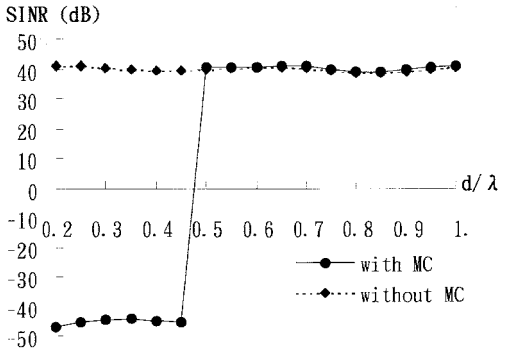

Fig. 5. The SINR patterns with respect to the interelement spacing, $\Phi_d = 90°$, and $\Phi_i = 40°$.

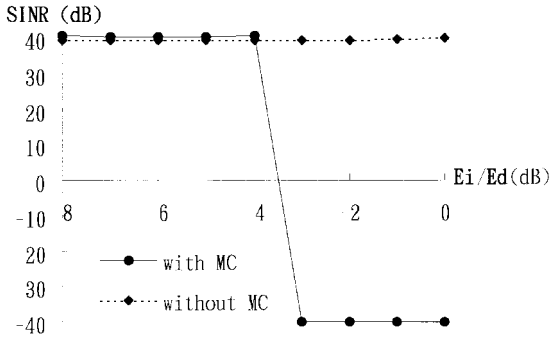

Fig. 6. The SINR patterns with respect to the relative amplitude of the delayed ray, where $\Phi_d = 90°$, $\Phi_i = 50°$, and $d = 0.5\lambda$.

MC when $\boldsymbol{d}$ varies from 0.2λ to 1λ when $\Phi_d = 90°$ and $\Phi_i = 40°$. It can be seen that when $\boldsymbol{d}$ is less than 0.5λ, the CMA adaptive array with MC catches the second ray, and when $\boldsymbol{d}$ is greater than 0.5λ, it catches the first ray, while without MC the array catches the first ray for all $\boldsymbol{d}$. The reason is that the peak direction of the initial receiving pattern with $W_0 = [1, 0, 0, 0]^T$ varies from 90° to 0° as $\boldsymbol{d}$ varies from 0.8 to 0.2 wavelength. When $d > 0.8\lambda$, the array also catches the first ray although the peak direction of the initial receiving pattern is not at 90° any more. This is because that the capture property of the CMA adaptive array with MC is not only dependent upon the initial received powers of the rays, but also upon the step size of the steepest descent method. From this figure, it is evident that when interelement spacing is smaller, MC affects the performance of the CMA adaptive array more.

Fig. 6 shows the SINR patterns with respect to the relative amplitude of the electric field of the delayed ray with and without MC. When the amplitude ratio $\boldsymbol{E_i/E_d}$ is smaller than -4 dB, the CMA adaptive array catches the first ray while it catches the second ray when $\boldsymbol{E_i/E_d}$ is greater than -3 dB with the consideration of MC, but without the consideration of MC, the array catches the first ray for all the value of $\boldsymbol{E_i/E_d} \leq 0$ dB. This result shows that the MC will not affect the capture property when the amplitude of the delayed ray is much less than that of the direct ray. The SINR patterns with respect to the delayed time of the delayed ray are shown in Fig. 7. From this figure, it is seen that the delayed time of the second ray has no effect on the capture property of the CMA adaptive array

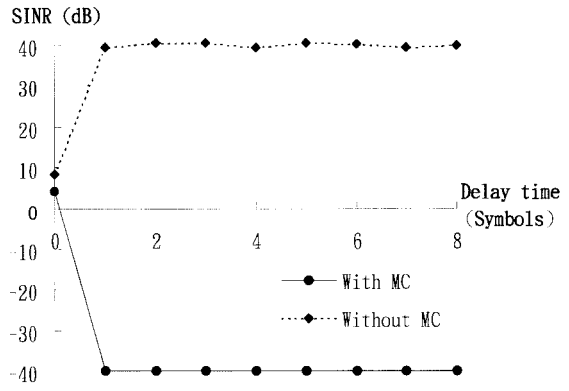

Fig. 7. The SINR patterns with respect to the delayed time, where $\Phi_d = 90°$, $\Phi_i = 50°$, $\boldsymbol{E_i}/\boldsymbol{E_d} = -2$ dB, and $d = 0.5\lambda$.

when the delayed time is greater than one symbol of the signal. When the delayed time is null, that is, the two rays are incident on the array synchronously, the CMA adaptive array does not work since in this case the multipath reception does not generate incidental amplitude fluctuations on the received signal.

From the analyses above, it is seen that with the consideration of MC, the CMA adaptive array sometimes catches the first ray and sometimes catches the second ray. Generally speaking, the array catching the second ray does not always mean an unfavorable condition if multipath propagation is well avoided to receive a single second ray, but in a practical mobile communication environment, a receiving system always moves and rotates. At one instant, the array is in the state of catching the first ray and suppressing the other one, and at another instant, the array may be in the state of catching the second ray and suppressing the first one as the receiving system rotates or the incident signals change the directions. The exchange of receiving states may cause some loss of information due to the delay time of the rays and the convergent speed of the algorithm. In this sense, the exchange of receiving states is unexpected and should be avoided. Also, catching a weaker ray may cause the degradation of the array performance, since the output SINR will be lower than that when catching a stronger one. From the simulations, we can see that the MC is one of the factors which can lead the array to catch a weaker ray instead of the stronger one. Besides, the MC will also affect the convergent speed of the CMA algorithm. Therefore, the consideration of MC is indispensable in the analysis of the CMA adaptive array antennas.

3) The Three-Ray Incidence: Now, we consider the case where there are three rays incident on the array. The first one is the direct ray and is also the desired ray. The other rays are delayed and undesired. The delay times of the second and third ray are T and $2T$ compared with the first one, respectively. The electric field amplitude ratio of the first ray to the second one is 3 dB and that to the third one is 6 dB. The incident directions of the three rays are $\Phi_d = 60°$, $\Phi_{i1} = 40°$, and $\Phi_{i2} = 110°$, respectively. The interelement spacing is 0.5λ, and the rest of the parameters are the same as those in the two-ray case. Fig. 8 shows the array output power with and without MC normalized by the initial output power of the first ray. It can be seen that the CMA array can also suppress the

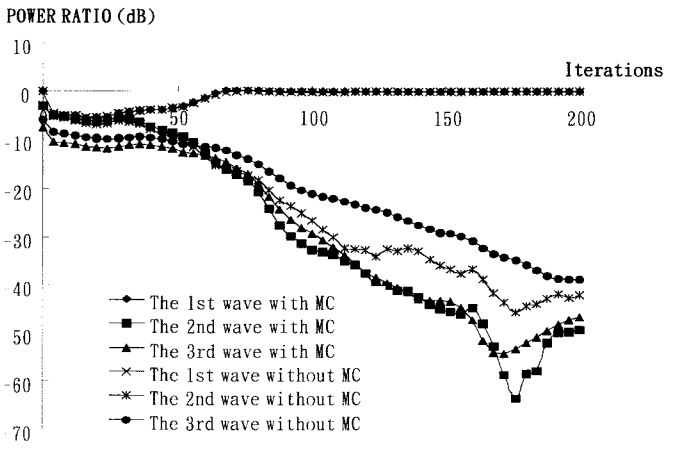

Fig. 8. The output power with respect to the number of iterations for three rays with and without MC, where $\Phi_d = 60°$, $\Phi_{i1} = 40°$, $\Phi_{i2} = 110°$, and $d = 0.5\lambda$.

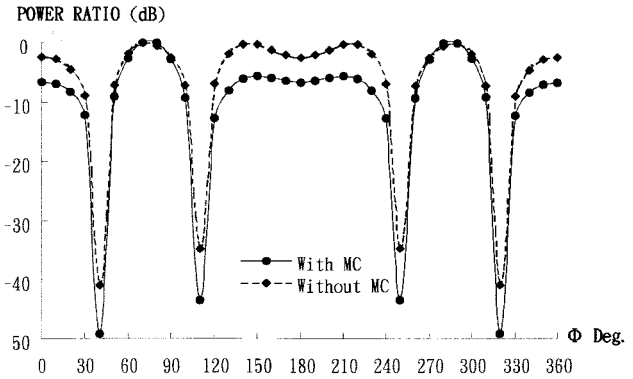

Fig. 9. The receiving patterns for three rays after 200 iterations of the CMA algorithm.

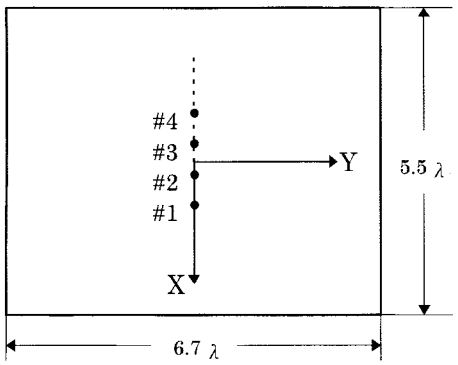

Fig. 10. The linear array on a finite rectangular conducting plate.

delayed rays more than one with MC. In this case, CMA has a faster convergence rate when MC is included.

Fig. 9 shows the receiving patterns for the three-ray incidence after 200 iterations of the CMA algorithm with and without MC. For each case, the pattern has deep nulls in the directions of the two delayed rays. Since in this case the CMA algorithm converges faster with MC, it suppresses the second and third ray more completely after 200 iterations (Fig. 8) compared with the one without MC. Therefore, the receiving pattern shows deeper nulls with MC than without MC.

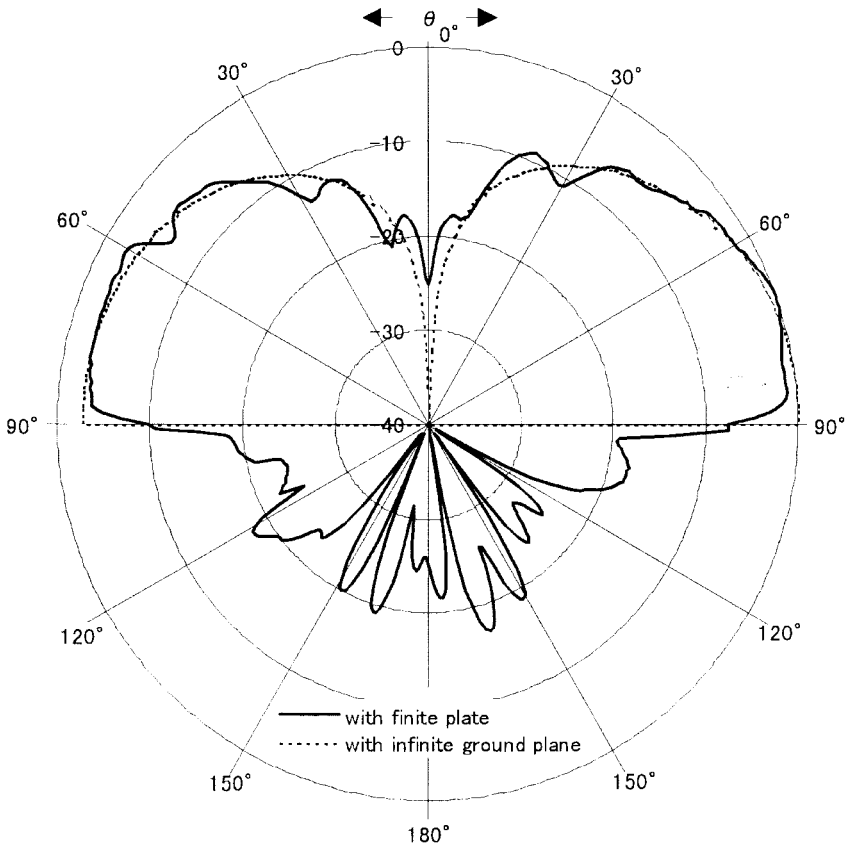

Fig. 11. The antenna pattern of the array in the $\Phi = 50°$ to $230°$ plane with initial element weights.

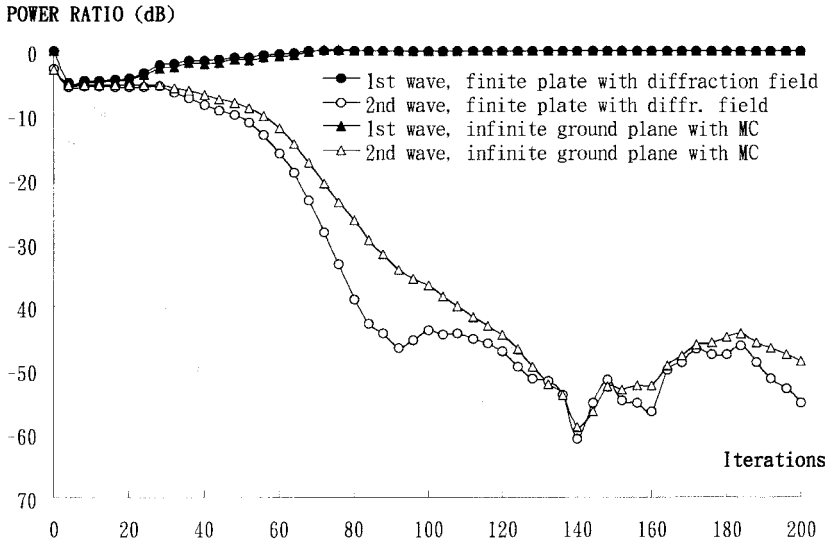

Fig. 12. The output power with respect to the number of iterations with the rectangular plate and the infinite ground plane when $\Phi_d = 90°$, $\theta_d = 80°$, $\Phi_i = 50°$, and $\theta_i = 70°$. $d = 0.5\lambda$.

B. CMA Adaptive Array on a Finite Rectangular Conducting Plate

In this section, the performance of a CMA adaptive array on a finite rectangular conducting plate is investigated and compared with that on an infinitely large ground plane. Consider an equally spaced linear array with four quarter-wavelength monopole antennas mounted on a rectangular conducting plate as shown in Fig. 10. The size of the plate is a $5.5\lambda \times 6.7\lambda$, which is the typical size of the car roof, and the array is mounted at the center of the plate. Fig. 11 shows the initial receiving patterns of the array in the $\Phi = 50°$ to $230°$ plane with the initial weight $W_0 = [1, 0, 0, 0]^T$ for the array on the finite plate and on an infinite ground plane, respectively. The two patterns differ, especially near $\boldsymbol{\theta} = 90°$. Since the performance of a CMA array is greatly affected by the initial received powers, it is assumed that the performance of a

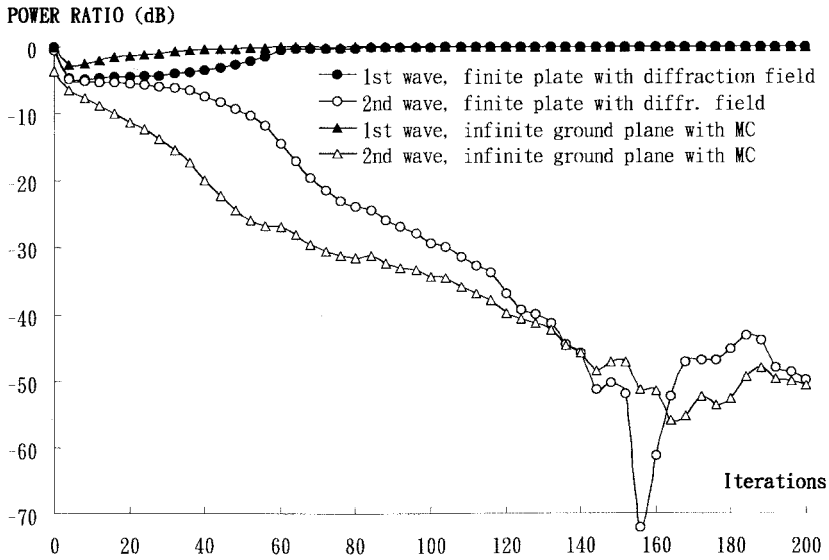

Fig. 13. The output power with respect to the number of iterations with the rectangular plate and the infinite ground plane when $\Phi_d = 110°$, $\theta_d = 80°$, $\Phi_i = 100°$, and $\theta_i = 65°$. $d = 0.5\lambda$.

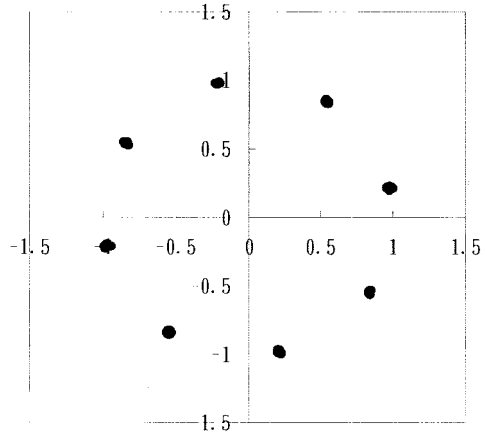

Fig. 14. The constellation pattern after convergence.

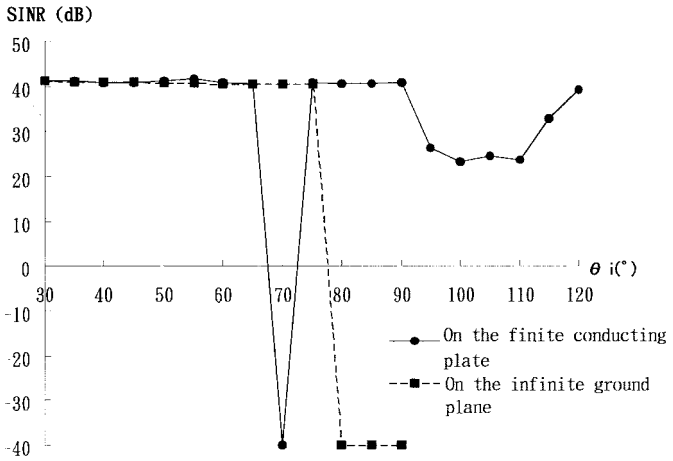

Fig. 15. SINR patterns with the finite and infinite planes after 200 iterations of the CMA algorithm when the first ray comes from $\Phi_d = 90°$ and $\theta_d = 80°$, and the second ray varies from $\theta_i = 30°$ to $120°$ in the $\Phi_i = 50°$ to $230°$ plane.

CMA adaptive array on the finite plate is different from that on the infinite ground plane. According to the experimental results reported in [15] and [16], the incident ray may arrive most probably from $30° \leq \theta \leq 90°$ in an urban area. Therefore, in this paper elevation angles between 0° and 60° ($30° \leq \theta \leq 90°$) are considered.

Figs. 12 and 13 show the array output power normalized by the initial output power of the first ray for the two-ray incidence case with and without the consideration of the rectangular plate when $d = 0.5\lambda$. Fig. 12 shows an example that when the first ray is incident from $\Phi_d = 90°$ and $\theta_d = 80°$, and the delayed ray from $\Phi_i = 50°$ and $\theta_i = 70°$, the convergent speed with the rectangular plate is faster than that with the infinite ground plane. Fig. 13 shows the reverse result, that is, when the first ray comes from $\Phi_d = 110°$ and $\theta_d = 80°$ and the second ray from $\Phi_i = 100°$ and $\theta_i = 65°$, the convergence rate of the array on the finite plate is slower than that on the infinite ground plane. This means that the diffracted field also affects the convergent speed of the CMA adaptive array.

Fig. 14 shows the constellation pattern after 100 iterations with the consideration of the diffraction by the rectangular plate. The incident directions are the same as in Fig. 12. It can be seen that the delayed ray has been suppressed completely.

Fig. 15 shows the SINR patterns after 200 iterations of the CMA algorithm with finite plate and infinite ground plane. The first ray is incident from $\Phi_d = 90°$ and $\theta_d = 80°$, while the incident direction of the delayed ray varies from $\theta_i = 30°$ to $\theta_i = 120°$ in the $\Phi_i = 50°$ to $230°$ plane. It can be seen that with infinite ground plane the array catches the first ray when $30° \leq \theta_i \leq 75°$, and it catches the second ray when $80° \leq \theta_i \leq 90°$. The reason why the array catches the second ray is the same as the explanation for Fig. 5, but with the finite plate, the array catches the first ray for all θ_i except at $\theta_i = 70°$. This is because the initial pattern has the maximum value at this angle. Since the initial received power at $\Phi_i = 50°$ is less than that at $\Phi_d = 90°$ with the

finite plate when $80° \leq \theta_i \leq 90°$, the array does not catch the second ray in this area. When $95° \leq \theta_i \leq 115°$, the SINR did not reach 40 dB after 200 iterations of the CMA algorithm. It is because the initial received power of the second ray is much less than that of the first ray, and this makes the steepest descent method converge slowly. The SINR reached 40 dB at $\theta_i = 120°$ because the initial SIR is already 40 dB. This point can be seen from Fig. 11. From Fig. 15 we can see that the diffracted field can also affect the capture property of the CMA adaptive array.

V. Conclusions

The performance of a CMA adaptive array with the consideration of MC effects among the array elements and the diffraction effects caused by the edges of a rectangular conducting plate was investigated. The performance of the CMA adaptive array is quite different with and without the MC effects. In some cases, the speed of convergence is slower with MC, and in other cases it is faster. Also, in multipath scenarios the array sometimes converges on a weaker delayed ray rather than the direct ray when MC is included. The capture property is explained by the fact that the CMA algorithm is sensitive to initial conditions and the initial array pattern is directional due to MC—not omnidirectional as in the ideal case. When the delayed ray is much weaker than the direct one, the MC will not affect the capture property of the array. Furthermore, the performance of the array is analyzed when the array is mounted on a rectangular plate. It can also be seen that the diffracted field caused by the edges of the finite plate not only affects the convergent speed of the CMA adaptive array, but affects the capture property as well. Since the exchange of receiving states may cause some loss of information due to the delay time of the rays or the convergent speed of the algorithm, it should be avoided in a practical mobile communication. Therefore, the consideration of MC and diffraction effects are indispensable in the analysis of the CMA adaptive array antennas.

Acknowledgment

The authors are grateful to M. Fujimoto at Toyota Central Research and Development Laboratory for his useful advice and discussion to this work.

References

[1] J. R. Treichler and B. G. Agee, "A new approach to multipath correction of constant modulus signals," *IEEE Trans. Acoust., Speech, Signal Processing*, vol. ASSP-31, pp. 459–472, Apr. 1983.
[2] B. Widrow *et al.*, "Stationary and nonstationary learning characteristics of the LMS adaptive filter," *Proc. IEEE*, vol. 64, pp. 1151–1162, Aug. 1976.
[3] R. Gooch and J. Lundell, "The CM array: An adaptive beamformer for constant modulus signals," in *Proc. IEEE ICASSP*, Apr. 1986, pp. 2523–2526.
[4] M. Fujimoto, N. Kikuma, and N. Inagaki, "Performance of CMA adaptive array optimized by Marquardt method for suppressing multipath waves," *Trans. IEICE Jpn*, vol. J 74-B-II, pp. 599–607, Nov. 1991.
[5] J. Perini and K. Hirasawa, "Antenna pattern distortion and mutual coupling in antenna farms," in *Proc. 1973 IEEE Int. Symp. Electromagnetic Compatibility*, June 1973, pp. 201–209.
[6] M. G. Larimore and J. R. Treichler, "Convergence behavior of the constant modulus algorithm," in *Proc. ICASSP*, Apr. 1983, pp. 13–16.
[7] W. L. Stutzman and G. A. Thiele, *Antenna Theory and Design.* New York: Wiley, 1981, pp. 500–502.
[8] D. M. Pozar and E. H. Newman, "Analysis of a monopole mounted near an edge or a vertex," *IEEE Trans. Antennas Propagat.*, vol. AP-30, pp. 401–408, May 1982.
[9] R. G. Kouyoumjian and P. H. Pathak, "A uniform geometrical theory of diffraction for an edge in a perfectly conducting surface," *Proc. IEEE*, vol. 62, pp. 1448–1461, Nov. 1974.
[10] W. L. Stutzman and G. A. Thiele, *Antenna Theory and Design.* New York: Wiley, 1981, pp. 472–476.
[11] E. P. Ekelman and G. A. Thiele, "A hybrid technique for combining the moment method treatment of wire antennas with the GTD for curved surfaces," *IEEE Trans. Antennas Propagat.*, vol. AP-28, pp. 831–839, Nov. 1980.
[12] C. A. Balanis, *Antenna Theory (Analysis and Design).* New York: Harper, 1982, pp. 510–515.
[13] A. R. Lopez, "The geometrical theory of diffraction applied to antenna pattern and impedance calculations," *IEEE Trans. Antennas Propagat.*, vol. AP-14, pp. 40–45, Jan. 1966.
[14] H. Yuan, K. Hirasawa, Y. Zhang, and M. Fujimoto, "The performance of the CMA adaptive array with mutual coupling consideration," in *Proc. 1995 Communications Society Conf. IEICE*, Sept. 1995, no. SB-1-1, pp. 335–336.
[15] F. Ikegami and S. Yoshida, "Analysis of multipath propagation structure in urban mobile radio environments," *IEEE Trans. Antennas Propagat.*, vol. AP-28, pp. 531–537, July 1980.
[16] Y. Asano *et al.*, "Estimation of incident waves' angular distribution in urban area," IEICE Technical Rep. AP88-127, pp. 41–46, Jan. 1989.

Hao Yuan was born in Henan, China, on February 25, 1961. He received the B.S. and M.S. degrees from Northwestern Polytechnical University, Xi'an, China, in 1981 and 1987, respectively, and the Ph.D. degree in electrical engineering from the University of Tsukuba, Tsukuba, Japan, in 1997.

From 1982 to 1995, he was with the Department of Applied Mathematics, Northwestern Polytechnical University, where he was a Lecturer in 1987. From 1991 to 1993, he was a Visiting Researcher at the Institute of Applied Physics, University of Tsukuba. From 1993 to 1997, he was at the Microwave Control Laboratory, Institute of Information Sciences and Electronics, University of Tsukuba. Currently, he is a Senior Researcher at the Kyocera DDI Institute of Future Telecommunications, Inc., Tokyo, Japan. His interests include mobile communications, adaptive array systems, and application of numerical techniques to antenna systems.

Dr. Yuan is a Member of the IEICE in Japan.

Kazuhiro Hirasawa (S'69–M'70) received the Ph.D. degree in electrical engineering from Syracuse University, Syracuse, NY, in 1971.

From 1967 to 1975, he was with the Department of Electrical and Computer Engineering, Syracuse University. From 1975 to 1977, he was a Consultant in the United States on the research and development of various antennas. Since 1978, he has been with the University of Tsukuba, Tsukuba, Japan. Currently, he is a Professor at the Institute of Information Sciences and Electronics. His current research interests include application of numerical techniques to antenna and electromagnetic compatibility problems. He is the coauthor of *Small Antennas* (Letchworth, U.K.: Research Studies Press, 1987), *Analysis, Design and Measurement of Small and Low-Profile Antennas* (Norwood, MA: Artech House, 1991), and *Small and Planar Antennas* (Tokyo, Japan: IEICE, 1996).

Yimin Zhang was born in Zhejiang, China, on December 27, 1964. He received the M.S. and Ph.D. degrees from the University of Tsukuba, Tsukuba, Japan, in 1985 and 1988, respectively.

Since 1988, he has been with the Department of Radio Engineering, Southeast University, Nanjing, China. He was a Foreign Research Fellow at the University of Tsukuba in 1989. From 1993 to 1995, he served as the General Manager of the Nanjing Oriental Environmental Protection Corporation, China. Currently, he is a Technical Manager at the Communication Laboratory, Japan Corporation, Kawasaki, Japan. His interests include adaptive arrays, mobile communications, and digital transmission in HDTV.

Dr. Zhang is a Member of IEICE in Japan.